ISSS Journal of Micro and Smart Systems
https://doi.org/10.1007/s41683-020-00061-2

SHORT COMMUNICATION

Semiconductor-based thermal wave crystals

Ahmed A. Zul Karnain[1] · Sai Aditya Raman Kuchibhatla[1] · Tiju Thomas[2] · Prabhu Rajagopal[1]

Received: 30 June 2020 / Revised: 2 September 2020 / Accepted: 25 September 2020

Abstract
One-dimensional phononic crystals made of silicon (Si) and germanium (Ge), both of which are materials commonly used in semiconductor devices, are shown to be effective in inducing bandgaps in the dispersion of heat flow at the nanoscale. Numerical approaches are used to understand the dispersion and propagation of thermal waves in Si–Ge phononic crystals. The results show for the first time how nanostructuring could yield band gaps in the dispersion of thermal phonons in the GHz range. We arrive at conditions that can yield bandgaps as high as 40 GHz; this is a bandgap that exceeds the value reported thus far. Variations in the unit cell dimensions are studied to understand the corresponding evolution in the bandgap frequencies. The control of heat using such proposed media holds promise for better heat management solutions for modern electronic devices, nanoscale sensing as well as for novel applications including the development of thermal diodes and thermal cloaks.

Keywords High band gap phononic crystals · Semiconductors · Thermal phonons · Thermal management

One of the critical issues affecting the reliability of electronic devices is the heating of components leading to malfunctions or impairment. With the ever-increasing demand for miniaturization and close packing, thermal management in today's devices, especially electronics, are of prime importance (Hannemann 2003). Particularly in crystalline materials, heat conduction is mediated primarily by phonons (quantized lattice vibrations) propagating through the lattice (Maldovan 2013a; Zhang et al. 2018; Nasri et al. 2015). At smaller length scales ($\sim$ nanometers) where the phonon wavelength is of the order of the lattice size, heat propagation becomes wave-like, in a quantum mechanical process known in the literature as 'second sound' (Chester 1963). Such phenomena are better modeled using the Cattaneo–Vernotte (CV) modification to heat transport, which is in the form of a hyperbolic partial differential equation (Tzou 2014; Glass et al. 1986; Marciak-Kozłowska 1994). Experimentally, the second sound has been observed in liquid helium (J. Donnelly R 2010), Bismuth (Narayanamurti and Dynes 1972), NaF (Pohl and Irniger 1976) and more recently in graphene (Huberman et al. 2019).

Our group has developed several phononic crystal and metamaterial concepts recently, enabling deep sub-wavelength imaging, extraordinary focusing, lensing and manipulation of elastic waves through phonon bandgap engineering (Amireddy et al. 2017, 2018; Kuchibhatla and Rajagopal 2019; Syed Akbar Ali et al. 2019; Manjunath and Rajagopal 2019). Indeed stop and pass bands within the transmission spectrum of phononic crystals and metamaterials have been widely studied in recent years to yield novel means to suppress or selectively allow the propagation of elastic waves (Mohammadi et al. 2007; Maldovan 2015; Colombi et al. 2015). Phononic crystals (and metamaterials) typically consist of repeating units (periodic or random sets of layers, cavities, inclusions etc.) of contrasting properties which contribute to band phenomena in the transmission spectrum. Several approaches (plane wave expansion, multiple scattering theory, finite difference in time domain calculations etc.) have been used to study the dispersion of waves within such media (Kushwaha et al. 1993; Sigalas and Economou 1993; Hussein et al. 2014; Kumar and Mitra 2012). Since the second sound is a wave-like phenomenon, it is posited that manipulation of heat in

✉ Prabhu Rajagopal
prajagopal@iitm.ac.in

[1] Centre for Nondestructive Evaluation, Department of Mechanical Engineering, Indian Institute of Technology Madras, Chennai, Tamil Nadu 600036, India

[2] DST Solar Energy Harnessing Center, and Department of Metallurgical and Materials Engineering, Indian Institute of Technology Madras, Chennai, Tamil Nadu 600036, India

Published online: 13 October 2020

suitable frequency regimes should be possible using thermal wave crystals (TWCs) made of appropriate materials (Maldovan 2015; Chen et al. 2018). However, no prior work has been reported for achieving TWCs yielding bandgaps in the GHz frequency range, which could spur interest for experimental device engineering. In a simple bilayer phononic crystal, the bandgaps or stop bands are formed due to local resonance and Bragg's scattering, i.e., due to destructive interference of waves scattered from boundaries between the layers. Developing TWCs with pass bands and stop bands at suitable frequencies offer the ability to selectively insulate regions up to varying degrees by modulating the passage of thermal phonons across the structure.

Here we explore commonly used semiconductor materials, silicon (Si) and germanium (Ge), for designing nanostructured one-dimensional (1D) TWCs (see Fig. 1 for an illustration) having bandgaps in the GHz range. Electronic components typically operate in the high MHz to GHz range, leading to the generation of heat (and hence thermal phonon phenomena) at such frequencies. Also, it is noted in the literature (see for example IP(Cook and Revier 2019)), that the wavelength of the phonons produced due to heating to 100 °C is about 2.5 nm which is within the range of unit layer dimensions of TWCs proposed here.

Si and Ge are also chosen as their combination to form super lattices, as has been reported in the literature on enhanced thermal conductivities in phononic structures (Slack 1964; Lin and Strachan 2013). As the Cattaneo–Vernotte (CV) model is the simplest of the candidates to represent hyperbolic heat conduction incorporating a wave-like behaviour, we consider this model for the mathematical treatment of wave propagation through the thermal wave crystals. The dispersion relation for heat waves is found using the transfer matrix method for a 1D TWC.

Transfer matrix simulations are carried out to study the propagation of temperature waves in the said TWC (Li 2001). This work offers insights on the range of properties, especially phonon relaxation time that need to be controlled to find applications in heat management of modern electronic devices.

The hyperbolic heat conduction equation in Eq. 1 considers the behaviour of thermal waves with finite speed and relaxation time-dependent attenuation leading to the emergence of bandgaps:

$$q + \tau_q \frac{\partial q}{\partial t} = -\kappa \frac{\partial T}{\partial x}, \tag{1}$$

here κ is the thermal conductivity, C is the heat capacity per unit volume which is equal to density ρ times the specific heat capacity c_p, and τ is the phonon relaxation time. The speed of a 'temperature wave' as per Eq. 1 is given by

$$C_{CV} = \sqrt{\frac{\kappa}{\rho c_p \tau_q}}. \tag{2}$$

Taking a time-harmonic assumption on the temperature, and considering the solution of Eq. 1 to be consisting of temperature waves travelling in both directions, an eigen value problem of the following form can be derived using the transfer matrix method (Chen et al. 2018). This derivation is explained in detail in Appendix 1 at the end of the article.

$$\cosh(ikl) = \cosh(i\gamma_A I_A)\cosh(i\gamma_B I_B) + \frac{1}{2}\left(\frac{\eta_A\gamma_A}{\eta_B\gamma_B} + \frac{\eta_B\gamma_B}{\eta_A\gamma_A}\right)\sinh(i\gamma_A I_A)\sinh(i\gamma_B I_B), \tag{3}$$

here l is the length, k is the wavenumber, $\gamma = \sqrt{\frac{\omega^2 + i\omega/\tau}{C_{CV}^2}}$ and $\eta = \frac{\kappa}{1 - i\omega\tau}$, the subscripts A and B represent two different materials. Numerical solution of Eq. 3 can be obtained by finding the complex wavenumber k for a given range of frequency ω. A purely imaginary wavenumber in a given frequency range indicates a band gap in the spectrum.

For validating our model, we have applied the above method for material properties [stratum-like (Layer A): thermal conductivity (W/m-K) = 0.235, specific heat (J/kg-K) = 3600, density (kg/m^3) = 1500, relaxation time (s) = 1, dermis-like (Layer B): thermal conductivity(W/m-K) = 0.445, specific heat (J/kg-K) = 3330, density (kg/m^3) = 1116, Relaxation time (s) = 20] and unit cell dimensions of 0.02 mm (each layer of 0.01 mm thickness) as mentioned in (Chen et al. 2018). Bandgaps were reported by them in the frequency intervals 1.8–3.5 Hz, 4.5–6.7 Hz and 7.9–9.3 Hz (Chen et al. 2018). The result obtained by our implementation of the transfer matrix method is shown in Fig. 2 (Chen et al. 2018). 'Pass bands' corresponds to the regions where the imaginary value of k is zero or very low. These regions allow the transmission of thermal waves with low losses. 'Bandgaps' corresponds to the region where the imaginary value of k is significantly higher, thus attenuating thermal waves of the frequency range. We can observe very similar results as obtained in (Chen et al. 2018), thus confirming our methodology. However, we note that the phonon relaxation times were

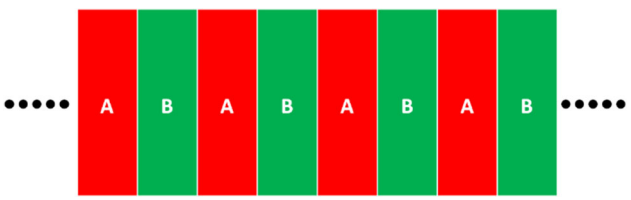

Fig. 1 Illustration of the architecture of a thermal wave crystal made by stacking layers with nanometer range thickness and alternating material properties (marked as A and B)

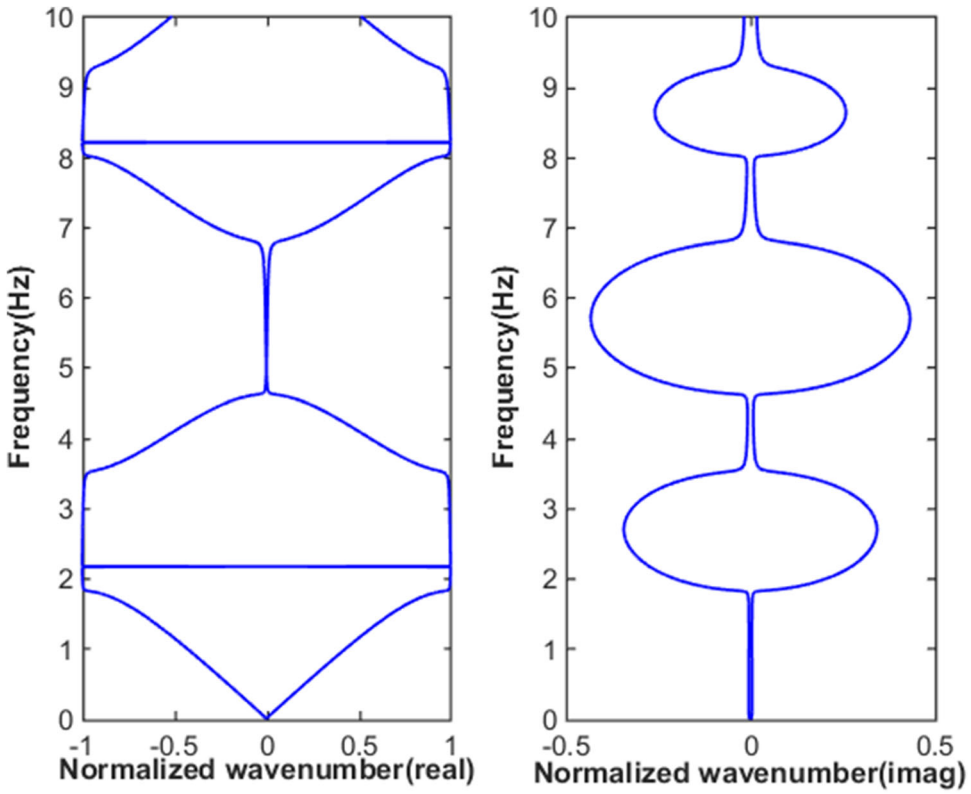

Fig. 2 Frequency vs. wavenumber (real and imaginary) shows bandgaps for properties mentioned in (Chen et al. 2018)

taken to be in the order of seconds in (Chen et al. 2018) and this is very difficult to realize in practice.

Considering that heat propagation occurs through high-frequency phonons (typically GHz range and above) (Maldovan 2013b; Kothari et al. 2019), we look for the creation of band gaps at frequencies above 1 GHz. First, we calculate the dispersion curves for an A–B type periodic structure with properties of A and B; set to be silicon and germanium (Periodictable 2020a, b; Henry and Chen 2008; Feng 2013) (ref: Table 1). The thickness of both Si and Ge layers are chosen to be 1 nm each, to begin with. The results of the calculation are shown in Fig. 3. The phonon relaxation time will vary for each phonon, as such the corresponding frequency of thermal wave packet will also vary considerably. However, we only consider the average phonon relaxation time instead of accounting for each phonon to simplify the model. This average phonon relaxation time was assigned based on the molecular dynamics (MD) simulations data obtained by Henry and Chen (2008) and Feng (2013). This average phonon relaxation time is dependent on temperature, amount of doping, boundary conditions and also other external factors.

Table 1 Material properties

Properties	Silicon	Germanium
Density (kg/m^3)	2330	5300
Thermal conductivity (W/m-K)	150	60
Specific heat (J/kg-K)	710	310
Phonon relaxation time (ps)	150[a]	200[a]

[a]Extrapolated from ref (Henry and Chen 2008; Feng 2013)

The central frequency of the band gap, calculated using Bragg scattering in the periodic structure like the one discussed here is given by Eq. 4 (Chen et al. 2018):

$$f = \frac{m}{2\left(\frac{l_A}{C_{CV_A}} + \frac{l_B}{C_{CV_B}}\right)}, \tag{4}$$

here A and B represent two different materials, l is the length, C_{CV} is the thermal wave speed as per the CV equation and m is a positive integer.

Based on Eq. 4, a 1 nm thick layer of each of the materials yields a centre frequency of the first bandgap at $\sim$ 140 GHz, which agrees well with results of our calculations, as shown in Fig. 3. The size of the bandgap is found to be 40 GHz. No previous literature has discussed achieving bandgaps at such high frequencies for phononic thermal transport phenomena. In IP (Cook and Revier 2019), the wavelength of phonons generated at 100 °C was mentioned to be 5 nm, which according to our method will correspond to a unit cell of similar size by invoking Braggs' scattering behaviour. Further, decreasing the

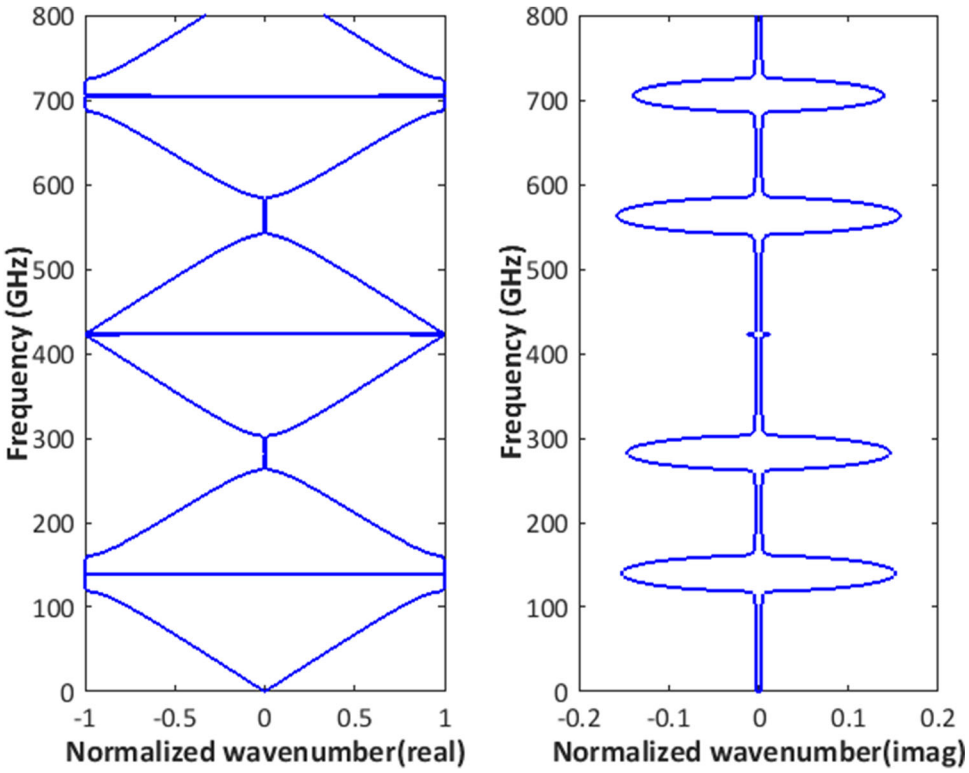

Fig. 3 Frequency vs. wavenumber (real and imaginary) shows bandgaps in regions where finite values of imaginary wavenumber exist for the unit cell chosen. The unit cell comprises of 1 nm thick Si layer followed by an equally thick Ge layer. 'Imaginary' wavenumbers indicate modes that attenuate

relaxation time leads to an increase in this frequency. It is possible to decrease the relaxation times within a given medium through techniques such as doping. This is done rather routinely in the manufacturing of semiconductors (Ho et al. 2008; Heremans et al. 2013). The dispersion curves in Fig. 4 show the dispersion curves obtained with variations in the length of the unit cell.

Calculations indicate that the first bandgap has a central frequency of $\sim$ 70 GHz. As we change the length of the unit cell to 2 nm each, we observe the shift in the central frequency of the band gap to 70 GHz, as shown in Fig. 4.

As shown in Fig. 5, the central frequency of the first phononic bandgap can be inferred to be decreasing with an increase in layer thickness. This is due to the increase in the length of the unit cell: as the wavelength of Bragg's scattering increases, the frequency of occurrence of band gap drops. Also, the decrease is steeper for Ge layers than for Si layers as the phonon velocity is higher in Ge than Si layer as (according to hyperbolic heat conduction theory) (Tzou 2014), as mentioned Eq. 2.

$$d(f) = \frac{-v}{\lambda^2} d(\lambda), \tag{5}$$

where f is the frequency of the phonon, v is phonon velocity and λ λ is the wavelength of the phonon. The length of the unit cell directly determines the wavelength of the band gap because of Bragg's scattering.

Indeed, thermal phonons may be of much higher frequencies than those discussed here. However, there exist methods to manipulate phonon frequencies associated with heat conduction by using discontinuities, impurities, guest atoms, dislocations etc. (Maldovan 2013b; Liu et al. 2018; Mingo et al. 2009). Hence TWCs such as the ones studied here could be indeed rendered useful for practical applications. Another variation on the TWC can be using polymers which have thermal properties for delivering switchable thermal bandgap (Zhou et al. 2018). A recent report shows the promise of the polymer polyvinylidene fluoride (PVDF) (Zhou et al. 2015). PVDF with periodic inclusions acting as phonon scattering centres could form a TWC useful for packaging applications in high-temperature conditions (Walker et al. 2019).

These insights offer exciting directions for application of results given here in practical electronic devices. IC chips on motherboards or PCBs are typically throttled by either drawn power or temperature (or both). But in these chips, when the rate of heat generation is higher than the heat taken out by the sink, it leads to an increase in the operating temperature of the chip and its environment. With the rise of highly intensive and parallel computing, the necessity for multichip configuration is on the rise. Figure 6a below presents a schematic of closely packed 4 chips/modules configurations that could make use of the proposed GHz range TWCs.

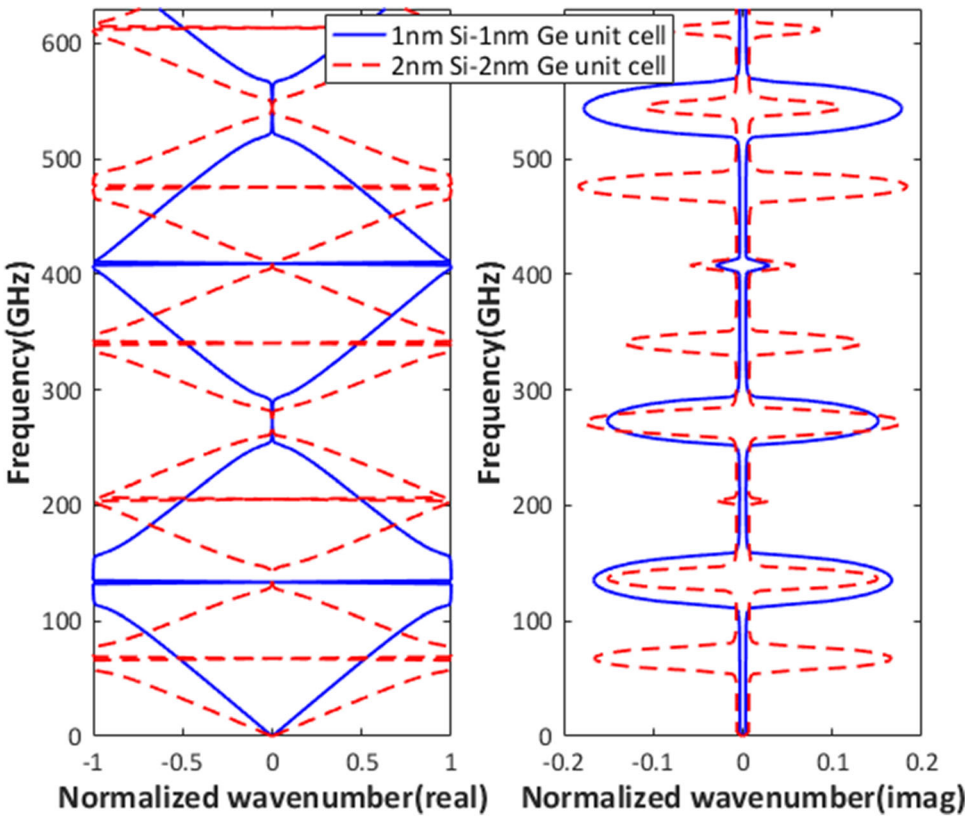

Fig. 4 Frequency Vs. wavenumber (real and imaginary) dispersion curves for unit cell cases with 1 nm Si −1 nm Ge and 2 nm Si −2 nm Ge

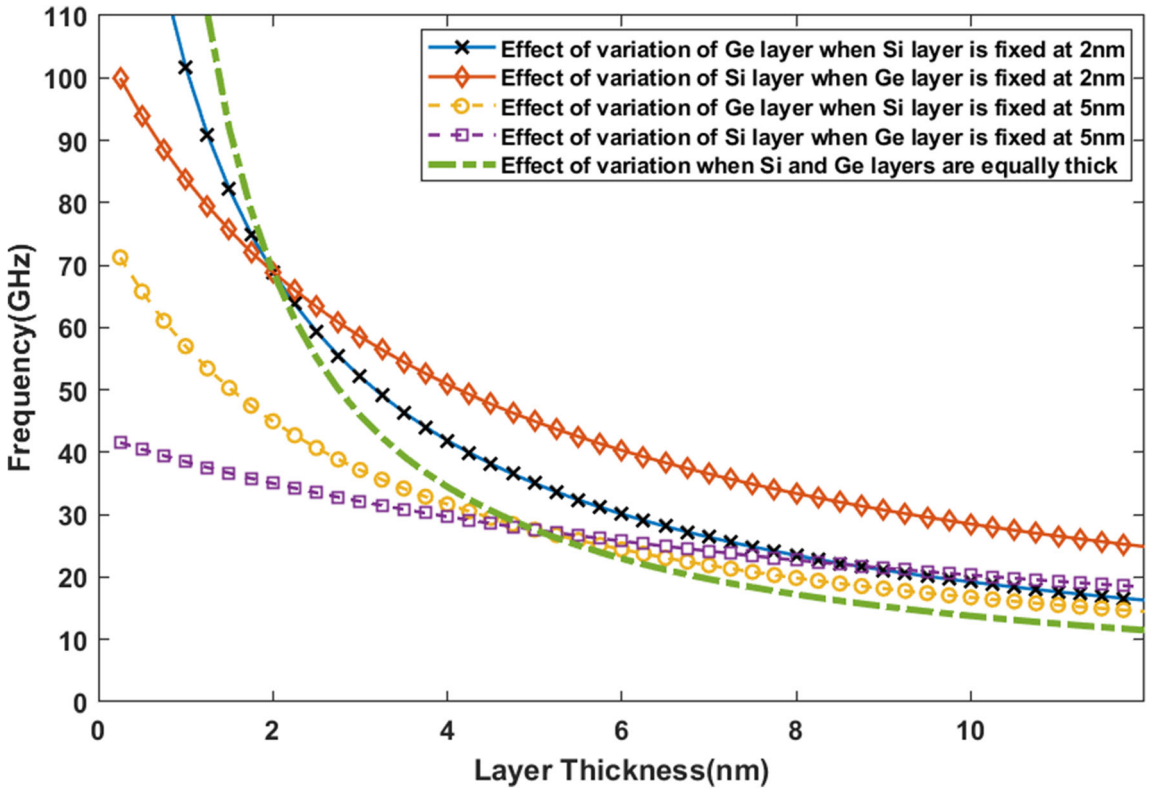

Fig. 5 Layer thickness Vs. central frequency of the first phononic bandgap for different cases of non-uniform layer thickness variation

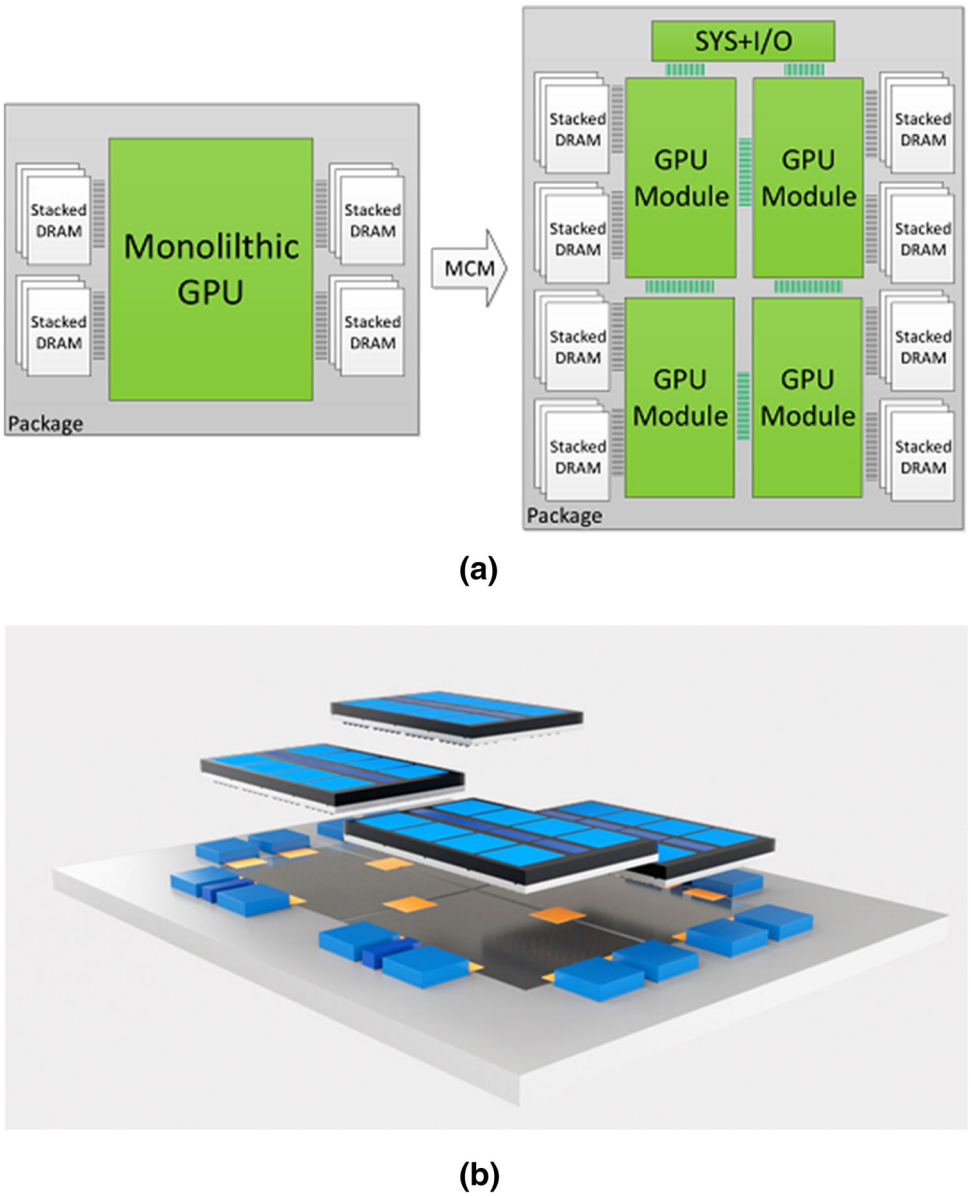

Fig. 6 **a** MCM-GPU: Aggregating GPU modules and DRAM on a single package (Arunkumar et al. 2017). **b** Illustration of 3D stacking architecture in Intel future generation of chips (Intel Foveros Interconnect 2019)

In a situation where a certain chip/module is fully loaded while the others are not, the former will eventually thermally throttle, ultimately compromising the performance of other chips as well. But placing our GHz TWCs phononic crystals as a buffer between the chips/modules could thermally insulate them, allowing for partial albeit lowered performance until at least one of them is operational. Where switching of chips/modules is allowed (for e.g. with the recent emphasis on 'chiplet' design by leading manufacturers), thermal insulation using our TWC could allow for loading particular chipsets/modules to full capacity until thermal limit where the operation can be switched to other chips/modules for full system utilization. Moreover, with the emphasis by leading chip designers and manufacturers such as Intel, AMD, Qualcomm etc. on the miniaturization of ICs, SOCs (System On Chips) and the development of 3D stacking of chips, (see for example Fig. 6b) our proposed TWCs will be of crucial importance.

In this paper, we discussed the possibility of achieving phononic bandgaps in dispersion curves associated with thermal wave crystal (TWC) made of widely used elemental semiconductor materials, silicon, and germanium. Dispersion curves obtained by employing the transfer matrix method indicate that the bandgap of approximately 40 GHz with a central frequency at 140 GHz exists for proposed nanostructured media (1 nm $-$ 1 nm layers). These bandgaps can be reduced by changing the lengths of the unit cell, and also by tailoring the phonon relaxation times in the material used. Manipulating the bandgaps at such high frequencies ($\sim$ GHz) and also lowering the

frequency of such bandgaps holds much promise for the development of artificial structures for modern electronic devices, nanoscale sensing as well as for novel applications including thermal diodes and thermal cloaks. Results mentioned in this paper open up a novel heat management technique in a wide range of applications such as electronics, nanostructures, energy harvesting, etc.

Appendix 1

The Catteneo–Vernotte (CV) heat conduction model in 1D can be written as

$$q + \tau_{\mathrm{q}} \frac{\partial q}{\partial t} = -\kappa \frac{\partial T}{\partial x}, \tag{6}$$

where q is the heat flux, T is the temperature,τ_{q} is the Phonon relaxation time, κ is the thermal conductivity.

The energy conservation equation with no internal heat generation is given by

$$\frac{\partial q}{\partial x} = -\rho c_{\mathrm{p}} \frac{\partial T}{\partial t}, \tag{7}$$

where ρ is the mass density, c_p is the specific heat.

Using Eqs. 6 and 7, we get the hyperbolic heat wave conduction equation for 1D, which is

$$\frac{1}{\tau_{\mathrm{q}}} \frac{\partial T}{\partial t} + \frac{\partial^2 T}{\partial t^2} = \frac{\kappa}{\rho c_{\mathrm{p}} \tau_{\mathrm{q}}} \frac{\partial^2 T}{\partial x^2}. \tag{8}$$

The propagation velocity (C_{CV}) of this thermal wave is given by

$$C_{\mathrm{CV}} = \sqrt{\frac{\kappa}{\rho c_{\mathrm{p}} \tau_{\mathrm{q}}}}. \tag{9}$$

A periodically layered 1D TWC structure is shown in Fig. 7. Each unit cell of thickness l consists of two layers A and B of thickness l_{A} and l_{B}, respectively. All the material properties of each layer are distinguished by subscript A and B while the left end and right end of the unit cell are represented by subscript L and R, respectively. The interface between the A and B layer is designated using the subscript AB. The superscript j represents the jth unit cell. The coordinate (x, y) are shown in Fig. 7.

$$l = l_{\mathrm{A}} + l_{\mathrm{B}}; x_{\mathrm{L}}^{\mathrm{j}} = jl; x_{\mathrm{AB}}^{\mathrm{j}} = jl + l_{\mathrm{A}}; x_{\mathrm{R}}^{j} = (j+1)l = x_{\mathrm{L}}^{j+1}. \tag{10}$$

Considering a 1D time-harmonic thermal wave propagating in the 1D periodic structure with angular frequency ω, the temperature and heat flux fields can be written as

$$\{T(x,t), q(x,t)\} = \left\{\hat{T}(x), \hat{q}(x)\right\} e^{-i\omega t}, \tag{11}$$

with $\hat{T}(x)$ satisfying

$$\hat{T}''(x) + \frac{\omega^2 + \frac{i\omega}{\tau_q}}{C_{CV}} \hat{T}(x) = 0, \tag{12}$$

where $i = \sqrt{-1}$.

The general solution of Eq. 12 is

$$\hat{T}(x) = A_1 e^{i\gamma x} + A_2 e^{-i\gamma x}, \tag{13}$$

where A_1 and A_2 are unknown coefficients, and

$$\gamma = \sqrt{\frac{\omega^2 + \frac{i\omega}{\tau_{\mathrm{q}}}}{C_{\mathrm{CV}}}}, \tag{14}$$

of which real part denotes propagating thermal wave while the imaginary part characterizes attenuation.

Using Eq. 7, we get

$$q(x) = -A_1 \frac{i\kappa\gamma}{1 - i\omega\tau_q} e^{i\gamma x} + A_2 \frac{i\kappa\gamma}{1 - i\omega\tau_q} e^{-i\gamma x}. \tag{15}$$

Introducing state vector,

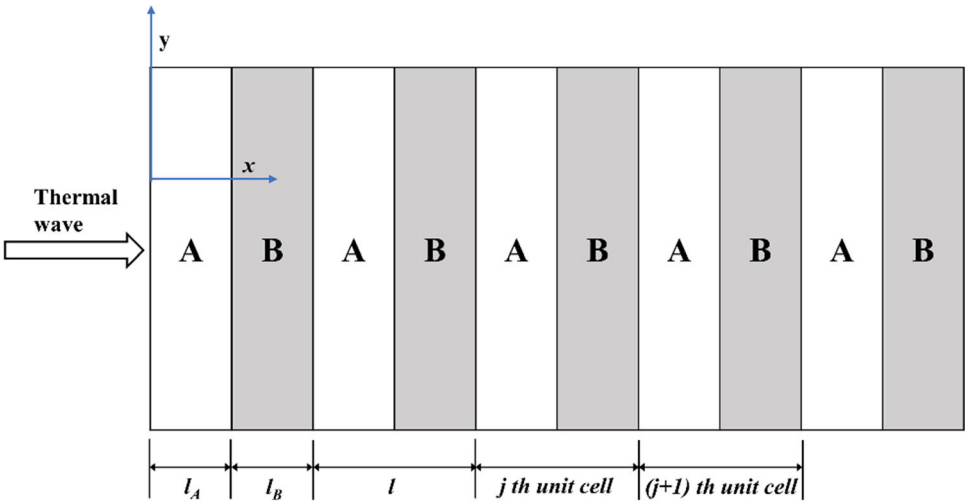

Fig. 7 Schematic of 1D periodic bilayer TWC

$$S(x) = \left\{ \hat{T}(x), \hat{q}(x) \right\}^T = M(x)\{A_1, A_2\}^T, \tag{16}$$

where

$$M(x) = \begin{pmatrix} -\dfrac{1}{i\kappa\gamma} & \dfrac{1}{i\kappa\gamma} \\ 1 - i\omega\tau_q & 1 - i\omega\tau_q \end{pmatrix} \begin{pmatrix} e^{i\gamma x} & 0 \\ 0 & e^{-i\gamma x} \end{pmatrix}. \tag{17}$$

The above solution is applicable for both layers A and B and is represented by $S_{\mathrm{A}}^j(x) = M_{\mathrm{A}}^j(x)\{A_1, A_2\}^T$(with $x_L^j < x < x_{\mathrm{AB}}^j$) in layer A and $S_{\mathrm{B}}^j(x) = M_{\mathrm{B}}^j(x)\{B_1, B_2\}^T$ (with $x_{\mathrm{AB}}^j < x < x_{\mathrm{R}}^j$) in layer B.

At the boundaries of layer A and B, state vectors can be written as

$$\begin{aligned} S_{\mathrm{AL}}^j &= M_{\mathrm{A}}^j(x_L^j)\{A_1, A_2\}^T; \quad S_{\mathrm{AR}}^j = M_{\mathrm{A}}^j(x_{\mathrm{AB}}^j)\{A_1, A_2\}^T \\ S_{\mathrm{BL}}^j &= M_{\mathrm{B}}^j(x_{\mathrm{AB}}^j)\{B_1, B_2\}^T; \quad S_{\mathrm{BR}}^j = M_{\mathrm{B}}^j(x_{\mathrm{R}}^j)\{B_1, B_2\}^T \end{aligned} \tag{18}$$

Eliminating $\{A_1, A_2\}^T$ and $\{B_1, B_2\}^T$, we get

$$S_{\mathrm{AR}}^j = M_{\mathrm{AR}}^j \left(M_{\mathrm{AL}}^j\right)^{-1} S_{\mathrm{AL}}^j; \quad S_{\mathrm{BR}}^j = M_{\mathrm{BR}}^j \left(M_{\mathrm{BL}}^j\right)^{-1} S_{\mathrm{BL}}^j \tag{19}$$

As temperature and heat flux are continuous at the interface between two adjacent sub-layers, we get

$$S_{\mathrm{AR}}^j = S_{\mathrm{BL}}^j; \quad S_{\mathrm{BR}}^j = S_{\mathrm{AL}}^{j+1}. \tag{20}$$

From Eq. 19 and 20, we get

$$\begin{aligned} S_{\mathrm{AL}}^{j+1} &= M_{\mathrm{BR}}^j \left(M_{\mathrm{BL}}^j\right)^{-1} M_{\mathrm{AR}}^j \left(M_{\mathrm{AL}}^j\right)^{-1} S_{\mathrm{AL}}^j, \\ S_{\mathrm{AL}}^{j+1} &= M_{\mathrm{Transfer}} S_{\mathrm{AL}}^j, \end{aligned} \tag{21}$$

where

$$M_{\mathrm{Transfer}} = M_{\mathrm{BR}}^j \left(M_{\mathrm{BL}}^j\right)^{-1} M_{\mathrm{AR}}^j \left(M_{\mathrm{AL}}^j\right)^{-1}$$

.

Using Bloch theorem, for a wave propagating through a periodic structure

$$S_{\mathrm{AL}}^{j+1} = e^{ikl} S_{\mathrm{AL}}^j. \tag{22}$$

here k is complex Bloch wavenumber and $k = k_{\mathrm{Re}} + k_{\mathrm{im}}$ (k_{Re} being the real part and k_{im} being the imaginary part).

Using Eqs. 21 and 22, we get

$$M_{\mathrm{Transfer}} S_{\mathrm{AL}}^j = e^{ikl} S_{\mathrm{AL}}^j, \tag{23}$$

or

$$\left| M_{\mathrm{Transfer}} - e^{ikl} I \right| = 0. \tag{24}$$

Using the detailed expression of M_{Transfer} in Eq. 24, we obtain the eigenvalue equation

$$\begin{aligned} \cosh(ikl) = {} & \cosh(i\gamma_{\mathrm{A}} I_{\mathrm{A}}) \cosh(i\gamma_{\mathrm{B}} I_{\mathrm{B}}) \\ & + \frac{1}{2}\left(\frac{\eta_{\mathrm{A}}\gamma_{\mathrm{A}}}{\eta_{\mathrm{B}}\gamma_{\mathrm{B}}} + \frac{\eta_{\mathrm{B}}\gamma_{\mathrm{B}}}{\eta_{\mathrm{A}}\gamma_{\mathrm{A}}} \right) \sinh(i\gamma_{\mathrm{A}} I_{\mathrm{A}}) \sinh(i\gamma_{\mathrm{B}} I_{\mathrm{B}}), \end{aligned} \tag{25}$$

where $\eta_{\mathrm{A}} = \frac{\kappa_{\mathrm{A}}}{\left(1 - i\omega\tau_{\mathrm{qA}}\right)}$ and $\eta_{\mathrm{B}} = \frac{\kappa_{\mathrm{B}}}{\left(1 - i\omega\tau_{\mathrm{qB}}\right)}$.

Solving Eq. 25, dispersion curves (ω vs k) for the 1D periodic TWC are obtained.

References

Amireddy KK, Balasubramaniam K, Rajagopal P (2017) Deep subwavelength ultrasonic imaging using optimized holey structured metamaterials. Sci Rep 7:1–8

Amireddy KK, Balasubramaniam K, Rajagopal P (2018) Porous metamaterials for deep sub-wavelength ultrasonic imaging. Appl Phys Lett 113:124102

Arunkumar A, Bolotin E, Cho B, Milic U, Ebrahimi E, Villa O, Jaleel A, Wu CJ, Nellans D (2017) MCM-GPU: multi-chip-module GPUs for continued performance scalability. ACM SIGARCH Comput Archit News 45:320–332

Available online at: https://periodictable.com/Elements/014/data.html. Last accessed 5 Jan 2020

Available online at: https://periodictable.com/Elements/032/data.html. Last Accessed 5 Jan 2020

Chen AL, Li ZY, Ma TX, Li XS, Wang YS (2018) Heat reduction by thermal wave crystals. Int J Heat Mass Transf 121:215–222

Chester M (1963) Second sound in solids physics. Phys Rev 132:2013–2015

Colombi A, Roux P, Guenneau S, Gueguen P, Craster RV (2015) Forests as a natural seismic metamaterial: Rayleigh wave bandgaps induced by local resonances. Sci Rep 6:19238

Cook BS, Revier DL (2019) Texas Instruments Incorporated (2019) Patent Application Publication (10) Pub . No.: US 2019 / 0094203 A1.1

Donnelly JR (2010) The two-fluid theory and second sound in liquid helium. Phys Today 62:34–39

Feng T (2013) Accurate prediciton of spectral phonon relaxation time and thermal conductivity of intrinsic and perturbed materials. Purdue University, Purdue

Glass DE, Özişik MN, McRae DS, Vick B (1986) Hyperbolic heat conduction with temperature-dependent thermal conductivity. J Appl Phys 59:1861–1865

Hannemann R (2003) Thermal control of electronics. Perspect Prospect 1–6.

Henry AS, Chen G (2008) Spectral phonon transport properties of silicon based on molecular dynamics simulations and lattice dynamics. J Comput Theor Nanosci 5:1–6

Heremans JP, Dresselhaus MS, Bell LE, Morelli DT (2013) When thermoelectrics reached the nanoscale. Nat Nanotechnol 8:471–473

Ho JC, Yerushalmi R, Jacobson ZA, Fan Z, Alley RL, Javey A (2008) Controlled nanoscale doping of semiconductors via molecular monolayers. Nat Mater 7:62–67

Huberman S, Duncan RA, Chen K, Song B, Chiloyan V, Ding Z, Maznev AA, Chen G, Nelson KA (2019) Observation of second sound in graphite at temperatures above 100 K. Science 364:375–379

Hussein MI, Leamy MJ, Ruzzene M (2014) Dynamics of phononic materials and structures: historical origins, recent progress, and future outlook. Appl Mech Rev 66:1–38

https://spectrum.ieee.org/tech-talk/semiconductors/processors/intel-shows-off-chip-packaging-powers(2019) Intel Foveros Interconnect.
Kothari K, Malhotra A, Maldovan M (2019) Cross-plane heat conduction in III–V semiconductor superlattices. J Phys Condens Matter 31:345301
Kuchibhatla SAR, Rajagopal P (2019) A transformation elasticity based device for wavefront manipulation. NDT E Int 102:304–310
Kumar V, Mitra M (2012) Vibration characteristics of periodically supported beam: application to railway track. In: 3rd ACMFMS International Conference
Kushwaha MS, Halevi P, Dobrzynski L, Djafari-Rouhani B (1993) Acoustic band structure of periodic elastic composites. Phys Rev Lett 71:2022
Li L (2001) MATLAB user manual. The MathWorks, Natick
Lin KH, Strachan A (2013) Thermal transport in SiGe superlattice thin films and nanowires: Effects of specimen and periodic lengths. Phys Rev B Condens Matter Mater Phys 87:1–9
Liu Z, Mao J, Liu TH, Chen G, Ren Z (2018) Nano-microstructural control of phonon engineering for thermoelectric energy harvesting. MRS Bull 43:181–186
Maldovan M (2013a) Sound and heat revolutions in phononics. Nature 503:209–217
Maldovan M (2013b) Narrow low-frequency spectrum and heat management by thermocrystals. Phys Rev Lett 110:1–5
Maldovan M (2015) Phonon wave interference and thermal bandgap materials. Nat Mater 14:667–674
Manjunath CT, Rajagopal P (2019) Lensing in the ultrasonic domain using negative refraction induced by material contrast. Sci Rep 9:1–8
Marciak-Kozłowska J (1994) Heat conduction in mesoscopic semiconductor structures. J Phys Chem Solids 55:721–726
Mingo N, Hauser D, Kobayashi NP, Plissonnier M, Shakouri A (2009) "Nanoparticle-in-alloy" approach to efficient thermoelectrics: silicides in SiGe. Nano Lett 9:711–715
Mohammadi S, Eftekhar AA, Khelif A, Moubchir H, Westafer R, Hunt WD, Adibi A (2007) Complete phononic bandgaps and bandgap maps in two-dimensional silicon phononic crystal plates. Electron Lett 43:898
Narayanamurti V, Dynes RC (1972) Observation of second sound in bismuth. Phys Rev Lett 28:1461–1465
Nasri F, Ben Aissa MF, Belmabrouk H (2015) Microscale thermal conduction based on Cattaneo–Vernotte model in silicon on insulator and Double Gate MOSFETs. Appl Therm Eng 76:206–211
Pohl DW, Irniger V (1976) Observation of second sound in NaF by means of light scattering. Phys Rev Lett 36:480–483
Sigalas M, Economou EN (1993) Band structure of elastic waves in two dimensional systems. Solid State Commun 86:141–143
Slack GA (1964) Thermal conductivity of Si and Ge. Phys Rev 134:10–13
Syed Akbar Ali MS, Amireddy KK, Balasubramaniam K, Rajagopal P (2019) Characterization of deep sub-wavelength sized horizontal cracks using holey-structured metamaterials. Trans Indian Inst Met 72:2917–2921
Tzou DY (2014) Macro to microscale heat transfer. Wiley, New York
Walker EL, Reyes-Contreras D, Jin Y, Neogi A (2019) Tunable hybrid phononic crystal lens using thermo-acoustic polymers. ACS Omega 4:16585–16590
Zhang L, Zhang X, Peng S (2018) Wave propagation model of heat conduction and group speed. Contin Mech Thermodyn 30:879–887
Zhou W, Wang Z, Dong L, Sui X, Chen Q (2015) Dielectric properties and thermal conductivity of PVDF reinforced with three types of Zn particles. Compos Part A Appl Sci Manuf 79:183–191
Zhou X, Chen J, Li Y, Sun Y, Xing Y (2018) Thermal tuning on band gaps of 2D phononic crystals considering adhesive layers. J Phys D Appl Phys 51:075105